

# An Improved Exact FBP Algorithm for Image Reconstruction in Cone-beam Helical CT

Jianhua Ma

School of Biomedical Engineering  
Southern Medical University  
Guangzhou, 510515, China  
Majh2005@fimmu.com

Wufan Chen

School of Biomedical Engineering  
Southern Medical University  
Guangzhou 510515, China  
Chenwf@fimmu.com

## Abstract

Recently, Katsevich proposed an exact FBP algorithm and its improved version for image reconstruction in helical cone-beam CT. In this paper, we present a new FBP image reconstruction algorithm by modifying Katsevich's original algorithm. This new algorithm is easier to implement and more efficient than the improved version of Katsevich's algorithm. Numerical simulations are performed to validate the proposed exact FBP algorithm. Results in these studies confirm the observation that the proposed algorithm can improve the image resolution over Katsevich's original algorithm with noiseless and noise projection data.

## 1. Introduction

In the last few years, significant progress has been achieved in image reconstruction from helical cone-beam projections. Investigation on stable and efficient algorithm for accurate reconstruction of images in helical cone-beam computed tomography (CT) has received much attention. Recently, Katsevich [2] [3] [4] proposed an elegant filtered backprojection (FBP) algorithm for accurate image reconstruction from helical cone-beam projection. In general, Katsevich's formula was basically published in a very general form that disregards the detector geometry. Later, Noo et al[5] presented a practical way that can be efficiently and accurately implement Katsevich's formula for direct reconstruction from data measured in two specific detector geometries. However, Noo's algorithm invokes a derivative along the helical trajectory and thus requires generally dense angular samples along the helical trajectory for retaining the resolution of the reconstructed images.

In this work, based upon Katsevich's original algorithm[4], we developed a new exact algorithm that can be easier to implement and more efficient than

the modified Katsevich's algorithm[5]. In our proposed algorithm, the reconstruction formula can be obtained by only computing the partial derivatives with respect to the coordinates on the detector plane. Although such a re-expression makes only a manipulation of mathematical variable, it may have a practical implication. Because the samples on a detector plane are generally much denser than are the angular samples in realistic cone-beam imaging situations. Therefore, the new expression formula can yield a numerically more accurate derivative of the data function than its direct calculation from the angular samples. Using such an expression for the angular derivative of the data function in equation, we obtain another algorithm for image reconstruction in a cone-beam scan. Numerical simulations presented in this paper have demonstrated that the performance of the proposed algorithm.

## 2. Background

### 2.1 Notations

The mathematical notations used throughout this paper will be introduced in this section. An image point inside a region of interest(ROI) is denoted as a vector  $\vec{x}$  or by its component  $\vec{x} = (x, y, z)^T$ . The density of the image object is denoted as  $f(\vec{x})$ , which is assumed to be confined within a support cylinder of radius  $R_0 < R$  with its central axis coinciding with that of the helix cylinder, as show in Fig.1. A helix in the 3D Cartesian coordinate system fixed on the object can be expressed as

$$\vec{y}(\lambda) = (R \cos \lambda, R \sin \lambda, \frac{h}{2\pi} \lambda)^T, \quad (1)$$

where  $h$  denotes the pitch length, which is the translation distance of the X-ray source along the  $z$ -axis between consecutive turns,  $R$  is the distance between the X-ray source and the rotation center,  $\lambda$  is the rotation angle. The

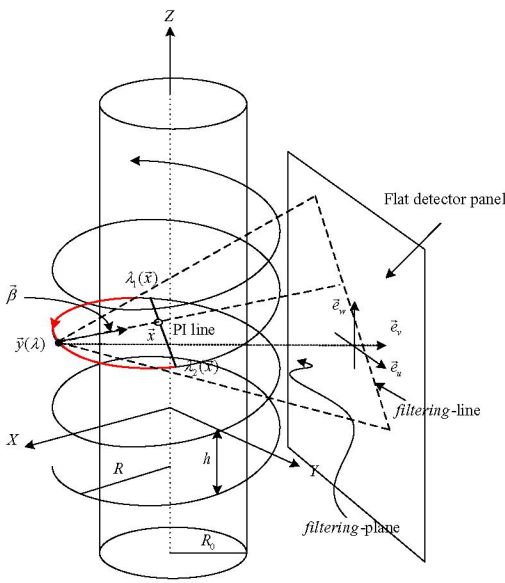


**Figure 1. Geometry of data acquisition with a flat detector plane.**

cone-beam projection of the object from the source point  $\vec{y}(\lambda)$  is written as

$$D(\vec{y}(\lambda), \vec{\beta}) = \int_0^\infty dt f(\vec{y}(\lambda) + t\vec{\beta}), \quad (2)$$

where  $\vec{\beta}(\lambda, \vec{x})$  denotes the unit vector that points to  $\vec{x}$  from the source  $\vec{y}(\lambda)$ , and is determined by

$$\vec{\beta} = \frac{\vec{x} - \vec{y}(\lambda)}{|\vec{x} - \vec{y}(\lambda)|}. \quad (3)$$

Following the notations used in [4], the normal vector to the plane containing  $\vec{\beta}$  may be parameterized by an angle  $\psi$  and denoted as  $\vec{n}(\lambda, \psi)$ . This plane will be denoted by  $\kappa(\lambda, \psi)$ , namely,  $\kappa$ -plane in this paper.

## 2.2 Katsevich algorithm

The Katsevich inversion formula is given by

$$\begin{aligned} f(\vec{x}) &= -\frac{1}{2\pi^2} \int_{I_{PI}(\vec{x})} \frac{1}{|\vec{x} - \vec{y}(\lambda)|} \\ &\times \int_0^{2\pi} \frac{\partial}{\partial q} D(\vec{x}(\lambda), \vec{\Theta}(\lambda, \vec{x}, \gamma))|_{q=\lambda} \frac{d\gamma d\lambda}{\sin \gamma}. \end{aligned} \quad (4)$$

where  $I_{PI} = [\lambda_1, \lambda_2]$  is the parametric interval corresponding to the unique PI-line [7] passing through  $\vec{x}$  and that

$\vec{\Theta}(\lambda, \vec{x}, \gamma) := \cos \gamma \vec{\beta}(\lambda, \vec{x}) + \sin \gamma \vec{e}(\lambda, \vec{x})$  and  $\vec{e}(\lambda, \vec{x}) := \vec{\beta}(\lambda, \vec{x}) \times \vec{n}(\lambda, \psi)$  lies in the appropriate  $\kappa$ -plane. Unit vector  $\vec{e}(\lambda, \vec{x})$  is in the plane determined by  $\vec{\beta}$  and  $\vec{y}'(\lambda) = \frac{d\vec{y}(\lambda)}{d\lambda}$  and perpendicular to  $\vec{\beta}(\vec{x}, \lambda)$ .

Katsevich proved that for a given  $\vec{x}$ , the  $\kappa$ -plane is uniquely determined if the projection of  $\vec{x}$  (called  $\hat{\vec{x}}$ ) onto the detector plane lies in the Tam-Danielsson window [6]. Let the  $\kappa$ -line be the line of intersection of the detector and a  $\kappa$ -plane. So if  $\hat{\vec{x}}$  lies in the Tam-Danielsson window, there is a unique  $\kappa$ -line.

Together,  $\kappa$ -lines and PI-lines obey the following important property. Consider a point  $\vec{x}$  within the field of view (FOV) and let  $\lambda_1, \lambda_2$  define the extremities of the PI-line through that point, with  $\lambda_1 < \lambda_2$ . For any  $\lambda \in [\lambda_1, \lambda_2]$ , there exists a  $\kappa$ -plane  $\kappa(\lambda, \psi)$  at  $\vec{y}'(\lambda)$  that contains  $\vec{x}$ . This property holds for any FOV size  $R_0 < R$ . See Katsevich (2003) for more details.

## 3 Reconstruction in the flat detector panel geometry

### 3.1 The helical cone-beam data function based on flat detector panel geometry

In the derivation of the new expression of Katsevich formula, it is useful to introduce a rotation-coordinate system  $(u, v, w)$ . For a rotation angle  $\lambda$ , we use unit vectors  $\vec{e}_u(\lambda)$ ,  $\vec{e}_v(\lambda)$  and  $\vec{e}_w(\lambda)$  to represent the directions of the three orthogonal axes  $u$ ,  $v$  and  $w$ , respectively, as shown in Fig. 1. In the fixed coordinate system  $(x, y, z)$ , the three unit vectors can be expressed as

$$\vec{e}_u(\lambda) = (-\sin \lambda, \cos \lambda, 0)^T \quad (5)$$

$$\vec{e}_v(\lambda) = (-\cos \lambda, -\sin \lambda, 0)^T \quad (6)$$

$$\vec{e}_w(\lambda) = (0, 0, 1)^T. \quad (7)$$

Clearly, unit vectors  $\vec{e}_u(\lambda)$  and  $\vec{e}_v(\lambda)$  are within the  $x$ - $y$  plane, whereas unit vector  $\vec{e}_w(\lambda)$  is along the  $z$ -axis. Therefore, unit vector  $\vec{e}_w(\lambda)$  can be interpreted as the normal vector of the detector plane. Additionally, any location within the detector plane can be characterized completely by a two-dimensional (2D) coordinate system  $(u, w)$  with its horizontal and vertical axes along  $\vec{e}_u(\lambda)$  and  $\vec{e}_w(\lambda)$ , respectively, and with its origin at the projection of the source point  $\vec{y}(\lambda)$  onto the detector plane.

Using the flat detector panel, the cone-beam projection appears as a function  $P(\lambda, u, w)$  in terms of the coordinates  $u$  and  $w$ , such that

$$P(\lambda, u, w) = D(\vec{y}(\lambda), \vec{\beta}), \quad (8)$$

$$u\vec{e}_u(\lambda) + w\vec{e}_w(\lambda) + D\vec{e}_v(\lambda) = A\vec{\beta}, \quad (9)$$

and  $A(u, w) = \sqrt{u^2 + w^2 + D^2}$ .

Conversely, for a direction  $\vec{\beta}$  pointing towards the detector panel

$$D(\vec{y}(\lambda), \vec{\beta}) = P(\lambda, u, w), \quad (10)$$

where

$$u = D \frac{\vec{\beta} \cdot \vec{e}_u(\lambda)}{\vec{\beta} \cdot \vec{e}_v(\lambda)} \quad w = D \frac{\vec{\beta} \cdot \vec{e}_w(\lambda)}{\vec{\beta} \cdot \vec{e}_v(\lambda)}. \quad (11)$$

### 3.2 Reconstruction formula in the flat detector panel geometry

Similarly the result of [5], Katsevich formula in the flat detector geometry can be expressed as

$$f(\vec{x}) = -\frac{1}{2\pi} \int_{\lambda_1(\vec{x})}^{\lambda_2(\vec{x})} d\lambda \frac{1}{|\vec{x} - \vec{y}(\lambda)|} g^F(\lambda, \vec{\beta}), \quad (12)$$

where  $\lambda_1$  and  $\lambda_2$  define the extremities of the PI-line through  $\vec{x}$  with  $\lambda_1 < \lambda_2$ ,  $g^F(\lambda, \vec{\beta})$  denotes the filtered data.

To obtain  $g^F(\lambda, \vec{\beta})$ ,  $\frac{\partial}{\partial \lambda} D(\vec{y}(\lambda), \vec{\beta})$  needs to be computed firstly. If we denote  $P(\lambda, u, w) = D(\vec{y}(\lambda), \vec{\beta})$  and  $\frac{\partial}{\partial \lambda} D(\vec{y}(\lambda), \vec{\beta}) = P_\lambda(\lambda, u, w)$  in the flat detector panel, then, applying the chain differentiation rule,  $P_\lambda(\lambda, u, w)$  can be expressed as

$$P_\lambda(\lambda, u, w) = \left( \frac{\partial P}{\partial \lambda} + \frac{D^2 + u^2}{D} \frac{\partial P}{\partial u} + \frac{uw}{D} \frac{\partial P}{\partial w} \right)(\lambda, u, w). \quad (13)$$

Hence, we have

$$g^F(\lambda, \vec{\beta}) = -\frac{1}{\vec{\beta} \cdot \vec{e}_v} g_{(f)}^F(\lambda, u, w), \quad (14)$$

$$g_{(f)}^F(\lambda, u, w) = \int_{-\infty}^{+\infty} du' h(u - u') \frac{D}{A(u, w)} P_\lambda(\lambda, u', w), \quad (15)$$

In this expression,  $h$  is the kernel of the Hilbert transform, i.e.  $h(s) = \frac{1}{\pi s}$ . The convolution needs to be computed in the proper  $\kappa$ -line using rebinning technique.

It can be observed that the algorithm based upon Eq.(15) calculates the derivative,  $\frac{\partial P(\lambda, u, w)}{\partial \lambda}$ , of the data along the helical trajectory. However, the accuracy of numerical calculation of such a derivative is highly dependent upon the sampling density along the helical trajectory. Katsevich developed an improved algorithm that is less sensitive to the computation of derivatives along the helical trajectory. Unfortunately, this algorithm contains five terms, which may cause the algorithm to be less easier to implement and less computationally efficient than the original algorithm in Eq.(4).

Function  $f(\vec{x})$  was obtained by use of backprojection of the corresponding filtered data  $g_{(f)}^F(\lambda, u, w)$ . Using the result in Eqs.(12-15), as show in Appendix, we obtain an inversion reconstruction formula in which all the derivatives

are performed with respect to the detector variables that contains only tree terms.

As is showed in Appendix, the new reconstruction algorithm can be expressed as

$$\begin{aligned} f(\vec{x}) &= \frac{1}{2\pi} \int_{\lambda_1(\vec{x})}^{\lambda_2(\vec{x})} d\lambda \frac{1}{|\vec{x} - \vec{y}(\lambda)|^2} \left( -\frac{\partial \vec{y}(\lambda)}{\partial \lambda} \cdot \vec{\beta} \right) \\ &\quad \times g_h^{(1)}(\lambda, u, w)_{\vec{\beta}} \\ &- \frac{1}{2\pi} \int_{\lambda_1(\vec{x})}^{\lambda_2(\vec{x})} d\lambda \frac{1}{|\vec{x} - \vec{y}(\lambda)|} g_h^{(2)}(\lambda, u, w)_{\vec{\beta}} \\ &- \frac{1}{2\pi} \frac{1}{|\vec{x} - \vec{y}(\lambda)|} g_h^{(1)}(\lambda, u, w)_{\vec{\beta}} \Big|_{\lambda_1(\vec{x})}^{\lambda_2(\vec{x})}, \end{aligned} \quad (16)$$

where  $g_h^{(1)}(\lambda, u, w)_{\vec{\beta}}$  and  $g_h^{(2)}(\lambda, u, w)_{\vec{\beta}}$  denote the filtered projection data in the direction of a projection ray at the unit vector  $\vec{\beta}$ .  $g_h^{(1)}(\lambda, u, w)$  and  $g_h^{(2)}(\lambda, u, w)$  are given by

$$g_h^{(1)}(\lambda, u, w) = \int_{-\infty}^{+\infty} du' h(u - u') \frac{D}{A(u, w)} P(\lambda, u, w), \quad (17)$$

$$\begin{aligned} g_h^{(2)}(\lambda, u, w) &= \int_{-\infty}^{+\infty} du' h(u - u') \frac{D}{A(u, w)} \\ &\quad \times \left( \frac{u^2 + D^2}{D} \frac{\partial P}{\partial u} + \frac{uw}{D} \frac{\partial P}{\partial w} \right)(\lambda, u, w), \end{aligned} \quad (18)$$

where

$$v_{\vec{\beta}} = R - x \cos(\lambda) - y \sin(\lambda), \quad (19)$$

$$u_{\vec{\beta}} = \frac{D}{v_{\vec{\beta}}} (-x \sin(\lambda) + y \cos(\lambda)), \quad (20)$$

$$w_{\vec{\beta}} = \frac{D}{v_{\vec{\beta}}} (z - \frac{h}{2\pi} \lambda). \quad (21)$$

Using the result of Eq.(16), the Katsevich's algorithm can be efficiently and accurately implemented by reducing the computational complexity. Although such a re-expression makes only a manipulation of mathematical variable, it may have a practical implication. The reason is that, in realistic cone-beam imaging situations, the samples on a detector plane are generally much denser than are the angular samples. Therefore, the new expression can yield a numerically more accurate derivative of the data function than its direct calculation from the angular samples. Using such an expression for the angular derivative of the data function in Eq.(16), we obtain another algorithm for image reconstruction in a cone-beam scan. In the following section, we will evaluate the performance of the proposed algorithms.

## 4 Numerical study

In this section, we present several numerical examples that illustrate the performance of the proposed 3D exact FBP algorithm compared to Katsevich's original algorithm. In our preliminary computer-simulation studies, we use the modified 3D Shepp-Logan phantom[1] to generate cone beam projection data, Table.1 contains the parameter values. Additional simulation parameters are presented in table 2. The derivative was computed using the difference of adjacent samples with the output placed at mid-location. The backprojection was implemented using a standard pixel-driven approach, with a linear interpolation approximated by pre-interpolating the projections by a factor of 2 and using nearest neighbours. For the Hilbert filtering step(Eqs.(17)(18)), the convolution using the Hilbert kernel was achieved using the FFT with a kernel that is a discretization of the analytic Fourier inversion of  $isgn(\omega)$  with a cut-off at the Nyquist frequency. For the implementation of the rebinning method to determine the filter line ( $\kappa$ -line) in Eqs.(17)(18), we use the linear interpolation. Fig.2

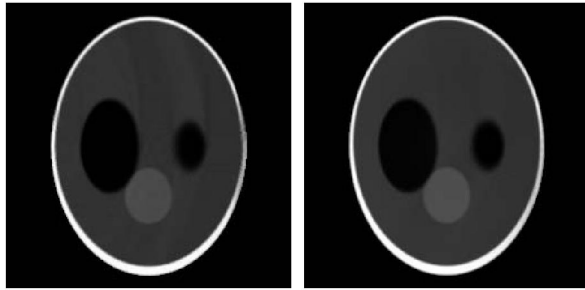


**Figure 2.** Images reconstructed by use of the Katsevich's algorithm (left) and the proposed FBP algorithm (right) at transverse slices specified by  $z = 0.1$ , respectively. The display grey scale is [0,1].

presents the reconstructed images on the left and right by use of Katsevich's original algorithm [4] and the proposed algorithm in Eq.(16), respectively. It can be seen that the resolution of the image on the right is better than that of the image on the left.

The results in Fig.3 are given to examine the stability of the proposed algorithm with respect to noise. The noisy projection data were generated from a Gaussian distribution with a zero mean and a standard deviation that is 0.1% of the maximum value in the noiseless projection data. From such noisy data, we use the proposed FBP algorithms and Katsevich's original algorithm to reconstruct the ROIs, which are displayed in Fig.3. These results again verify our theoretical prediction that the proposed algorithm in Eq.(16) produced

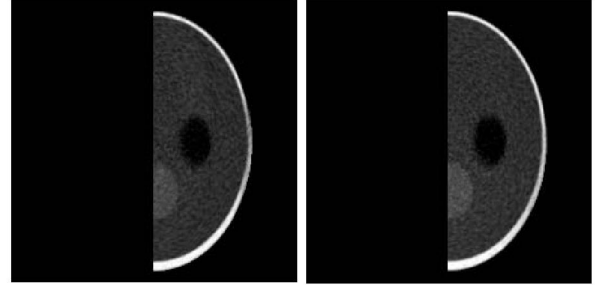


**Figure 3.** Images reconstructed by use of the Katsevich's original algorithm(left) and the proposed FBP algorithm(right) at transverse slices specified by  $z = 0.1$ , respectively, from data containing Gaussian noise. The display grey scale is [0,1].

the better numerically stable than the Katsevich's original algorithm.

**Table 1. Parameters of the modified 3D Shepp-Logan phantom data**

No.	A	a	b	c	$x_0$	$y_0$	$z_0$	$\varphi$	$\theta\psi$
1	1	0.6900	0.9200	0.8100	0	0	0	0	00
2	-0.8	0.6624	0.8740	0.7800	0	-0.0180	0	0	00
3	-0.2	0.1100	0.3100	0.2200	0.220	0	0	-18	010
4	-0.2	0.1600	0.4100	0.2800	-0.2200	0	0	0	010
5	0.1	0.2100	0.2500	0.4100	0	0.350	-0.1500	0	00
6	0.1	0.0460	0.0460	0.0500	0	0.100	0.250	0	00
7	0.1	0.0460	0.0460	0.0500	0	-0.100	0.250	0	00
8	0.1	0.0460	0.0230	0.0500	-0.080	-0.6050	0	0	00
9	0.1	0.0230	0.0230	0.0200	0	-0.6060	0	0	00
10	0.1	0.0230	0.0460	0.0200	0.060	-0.6050	0	0	00

## 5 Conclusion

We have presented a new exact 3D FBP algorithm for image reconstruction from helical cone-beam projection data. From visual inspection of images reconstructed from projections with and without noise, the proposed algorithm appears to perform very well, and with comparable computational efficiency. In realistic cone-beam imaging situations, the discrete projection data on a detector plane are generally much denser than are the angular samples. When applied to reconstructing images from projection data, the new algorithm can make a numerically more accurate derivative of the data function than its direct cal-

**Table 2. Simulation and reconstruction parameters.**

Parameters	Values	Units
Number of detectors per rows	16	
Number of detectors per cols	276	
h (pitch of the spiral)	1.56	cm
Detector element height	1.5	mm
Detector element width	1.5	mm
Source-to-detector distance(Ro)	100	cm
Source-to-rotation-axis distance(D)	50	cm
Number of projection per turn	360	

culation from the angular samples and yields images with better resolution than does Katsevich's original algorithm. Because this algorithm involves data operations on the detector plane, it is easier to implement than is Katsevich's original algorithm. The simulations presented in this paper have demonstrated that the performance of the proposed algorithm.

## 6 Acknowledgements

This work was supported by 973 Program of China (No: 2003CB716101).

## References

- [1] A.C.Kak and M. Slaney. *Principles of Computed Tomography Imaging*. IEEE Bellingham, WA., 1988.
- [2] A.Katsevich. Analysis of an exact inversion algorithm for spiral cone-beam ct. *Phys.Med.Biol.*, 47:2583–2598, 2002.
- [3] A.Katsevich. Theoretically exact filtered backprojection-type inversion algorithm for spiral ct. *SIAM J.Appl.Math.*, 62:2012–2026, 2002.
- [4] A.Katsevich. An improved exact filtered backprojection algorithm for spiral computed tomography. *Advances in Applied Mathematics*, 32:681–697, 2004.
- [5] J. F.Noo and D.Heuscher. Exact helical reconstruction using native cone-beam geometries. *Phys.Med.Biol.*, 48:3787–3818, 2003.
- [6] K.C.Tam. Exact local region-of-interest reconstruction in spiral cone-beam filtered backprojection ct: theory. *Proc.SPIE Medical Imaging*, 3979:506–519, 2000.
- [7] P. E. P.E.Danielsson and M.Seger. Towards exact 3d-reconstruction for helical cone-beam scanning of long objects. a new detector arrangement and a new completeness condition. in *Proceedings of the 1997 International Meeting on Fully Tree-Dimensional Image Reconstruction in Radiology and Nuclear Medicine*, pages 141–144, 1997.
- [8] Y.Zou and X.Pan. Exact image reconstruction on pi-lines from minimum data in helical cone beam ct. *Phys.Med.Biol.*, 49:941–959, 2004.

- [9] Y.Zou and X.Pan. Three-term exact fbp reconstruction in cone-beam helical ct. *IEEE Medical Imaging Conference Record*, pages 2735–2738, 2004.

## Appendix: Derivation of the formula Eq.(16)

In this appendix, we show how to derive reconstruction formula Eq.(16). Denote,

$$\begin{aligned} \tilde{g}_h^{(1)}(\lambda, u, w) &= \int_{-\infty}^{+\infty} du' h(u - u') \frac{D}{A(u, w)} \frac{\partial P(\lambda, u, w)}{\partial \lambda} \\ &= \frac{\partial}{\partial \lambda} \int_{-\infty}^{+\infty} du' h(u - u') \frac{D}{A(u, w)} P(\lambda, u, w), \end{aligned} \quad (22)$$

$$\begin{aligned} g_h^{(2)}(\lambda, u, w) &= \int_{-\infty}^{+\infty} du' h(u - u') \frac{D}{A(u, w)} \\ &\times \left( \frac{u^2 + D^2}{D} \frac{\partial P}{\partial u} + \frac{uw}{D} \frac{\partial P}{\partial w} \right)(\lambda, u, w). \end{aligned} \quad (23)$$

Using Eqs.(12-15), we obtain

$$\begin{aligned} f(\vec{x}) &= -\frac{1}{2\pi} \int_{\lambda_1(\vec{x})}^{\lambda_2(\vec{x})} d\lambda \frac{1}{|\vec{x} - \vec{y}(\lambda)|} g_{(f)}^F(\lambda, u, w)_{\beta} \\ &= -\frac{1}{2\pi} \int_{\lambda_1(\vec{x})}^{\lambda_2(\vec{x})} d\lambda \frac{1}{|\vec{x} - \vec{y}(\lambda)|} \tilde{g}_h^{(1)}(\lambda, u, w)_{\beta} \\ &- \frac{1}{2\pi} \int_{\lambda_1(\vec{x})}^{\lambda_2(\vec{x})} d\lambda \frac{1}{|\vec{x} - \vec{y}(\lambda)|} g_h^{(2)}(\lambda, u, w)_{\beta}. \end{aligned} \quad (24)$$

Denote,

$$g_h^{(1)}(\lambda, u, w) = \int_{-\infty}^{+\infty} du' h(u - u') \frac{D}{A(u, w)} P(\lambda, u, w). \quad (25)$$

Substituting the above equation into the first term of the Eq.(24) and integrating by parts with respect to  $\lambda$ , one obtains

$$\begin{aligned} &- \frac{1}{2\pi} \int_{\lambda_1(\vec{x})}^{\lambda_2(\vec{x})} d\lambda \frac{1}{|\vec{x} - \vec{y}(\lambda)|} \frac{\partial}{\partial \lambda} g_h^{(1)}(\lambda, u, w)_{\beta} \\ &= -\frac{1}{2\pi} \frac{1}{|\vec{x} - \vec{y}(\lambda)|} g_h^{(1)}(\lambda, u, w)_{\beta} \Big|_{\lambda_1(\vec{x})}^{\lambda_2(\vec{x})} \\ &+ \frac{1}{2\pi} \int_{\lambda_1(\vec{x})}^{\lambda_2(\vec{x})} d\lambda \frac{1}{|\vec{x} - \vec{y}(\lambda)|^2} \frac{(\vec{x} - \vec{y}(\lambda)) \cdot \left( -\frac{\partial \vec{y}(\lambda)}{\partial \lambda} \right)}{|\vec{x} - \vec{y}(\lambda)|} \\ &\quad \times g_h^{(1)}(\lambda, u, w)_{\beta} \\ &= -\frac{1}{2\pi} \frac{1}{|\vec{x} - \vec{y}(\lambda)|} g_h^{(1)}(\lambda, u, w)_{\beta} \Big|_{\lambda_1(\vec{x})}^{\lambda_2(\vec{x})} \end{aligned}$$

$$\begin{aligned}
& + \frac{1}{2\pi} \int_{\lambda_1(\vec{x})}^{\lambda_2(\vec{x})} d\lambda \frac{1}{|\vec{x} - \vec{y}(\lambda)|^2} \left( -\frac{\partial \vec{y}(\lambda)}{\partial \lambda} \cdot \vec{\beta} \right) \\
& \quad \times g_h^{(1)}(\lambda, u, w)_{\vec{\beta}} \tag{26}
\end{aligned}$$

where  $g_h^{(1)}(\lambda, u, w)_{\vec{\beta}}$  and  $g_h^{(2)}(\lambda, u, w)_{\vec{\beta}}$  denote the filtered projection data in the direction of a projection ray at the unit vector  $\vec{\beta}$ .

Substituting Eq.(26) into Eq.(24), we obtain a new inversion formula in which all the derivatives are performed with respect to the detector variables.

$$\begin{aligned}
f(\vec{x}) &= \frac{1}{2\pi} \int_{\lambda_1(\vec{x})}^{\lambda_2(\vec{x})} d\lambda \frac{1}{|\vec{x} - \vec{y}(\lambda)|^2} \left( -\frac{\partial \vec{y}(\lambda)}{\partial \lambda} \cdot \vec{\beta} \right) \\
&\quad \times g_h^{(1)}(\lambda, u, w)_{\vec{\beta}} \\
&- \frac{1}{2\pi} \int_{\lambda_1(\vec{x})}^{\lambda_2(\vec{x})} d\lambda \frac{1}{|\vec{x} - \vec{y}(\lambda)|} g_h^{(2)}(\lambda, u, w)_{\vec{\beta}} \\
&- \frac{1}{2\pi} \frac{1}{|\vec{x} - \vec{y}(\lambda)|} g_h^{(1)}(\lambda, u, w)_{\vec{\beta}} \Big|_{\lambda_1(\vec{x})}^{\lambda_2(\vec{x})}, \tag{27}
\end{aligned}$$

where

$$\begin{aligned}
v_{\vec{\beta}} &= -|\vec{x} - \vec{y}(\lambda)| \\
&= (\vec{x} - \vec{y}(\lambda)) \cdot \vec{e}_v(\lambda) \\
&= R - x \cos(\lambda) - y \sin(\lambda), \\
u_{\vec{\beta}} &= D \frac{< \vec{\beta}, \vec{e}_u >}{< \vec{\beta}, \vec{e}_v >} \\
&= D \frac{< \vec{x} - \vec{y}(\lambda), \vec{e}_u >}{< \vec{x} - \vec{y}(\lambda), \vec{e}_v >} \\
&= \frac{D}{v_{\vec{\beta}}} (-x \sin(\lambda) + y \cos(\lambda)), \\
w_{\vec{\beta}} &= D \frac{< \vec{\beta}, \vec{e}_w >}{< \vec{\beta}, \vec{e}_v >} \\
&= D \frac{< \vec{x} - \vec{y}(\lambda), \vec{e}_w >}{< \vec{x} - \vec{y}(\lambda), \vec{e}_v >} \\
&= \frac{D}{v_{\vec{\beta}}} \left( z - \frac{h}{2\pi} \lambda \right).
\end{aligned}$$